Ji, Yuan; Ge, Lei; Wang, Jiangpeng; Chen, Quangang; Wu, Wen

Differentially-Fed Aperture-Coupled Magneto-Electric Dipole Antenna With Continuously Variable Beamwidth

Published in:
IEEE Open Journal of Antennas and Propagation

DOI:
10.1109/OJAP.2020.2987929

Published: 01/01/2020

Document Version
Publisher's PDF, also known as Version of record

Received 1 February 2021; revised 12 March 2021; accepted 14 March 2021. Date of publication 19 March 2021; date of current version 29 March 2021.

Digital Object Identifier 10.1109/OJAP.2021.3067435

A Method for Tailoring the Gain Pattern of a Single Antenna Element

RIKU KORMILAINEN, ANU LEHTOVUORI, AND VILLE VIIKARI (Senior Member, IEEE)

Department of Electronics and Nanoengineering, Aalto University School of Electrical Engineering, 02150 Espoo, Finland

CORRESPONDING AUTHOR: R. KORMILAINEN (e-mail: riku.kormilainen@aalto.fi)

The work of Riku Kormilainen was supported by the Aalto ELEC Doctoral School.

ABSTRACT In this paper, we present a novel method to tailor the radiation pattern of an antenna element, such as a single element of an array, by maximizing its partial radiation efficiency in the desired angular space. The tailored pattern of the single element is achieved by current distribution synthesis using multiple feed points in the antenna. A method to determine and realize the currents at the feeds is presented. The method is demonstrated by designing and manufacturing a four-element linear array consisting of tailored antenna elements and comparing its performance to the reference case. The element consists of four closely-spaced metallic patches placed on a substrate backed with a ground plane, and each patch is separately fed. The initial four-port feed is reduced to a single feed with a feeding network based on the determined currents. A conventional patch antenna is chosen as the reference. The simulated and measured results show improvement in the realized gain in the desired angular space.

INDEX TERMS Antenna arrays, antenna efficiency, antenna feeds, antenna gain, antenna radiation pattern synthesis, design methodology.

I. INTRODUCTION

ANTENNA arrays are currently employed in a wide range of applications because of their directive properties. Examples of such applications include radars and emerging 5G technology, where large arrays are deployed to steer the radiation to a desired direction.

Traditionally, antenna array design has concentrated on array-level design, so as to reduce mutual coupling between elements, reduce the number of elements in the antenna array and optimize the array pattern, that is, the resulting pattern of the array. However, considering the single-element pattern is equally important since it defines the limitations of the antenna array. For example, a patch antenna has maximum gain in the broadside direction with relatively narrow half-power beamwidth. Hence, a patch antenna array suffers from significant scan loss and even scan blindness at large steering angles. Similarly, no canonical antenna in an array is well suited for beam steering across an arbitrary angular space.

Currently, there are a variety of studies that consider the element pattern as part of the array design. The first design option is to widen the single-element pattern to achieve larger steering range [1]–[6]. The other option is to use pattern-reconfigurable elements [7]–[11] for larger beam steering range in the vertical plane $\theta = [-90°, +90°]$. Arrays with wide element patterns are limited to spacings below 0.5λ to avoid emergence of grating lobes [10]. They can be avoided with pattern-reconfigurable elements since the single element does not radiate towards the grating lobes, which arise from the shape of the array factor.

However, in some cases the array does not necessarily need to radiate across the entire vertical range. In cellular communication, base station antennas typically serve users below them. Then, only a steering range of $\theta = [0°, 90°]$ may suffice. One possible example of this steering range requirement is an indoor access point antenna that should provide coverage to the whole room. Another example could be an outdoor base station antenna in a high-rise tower that should provide an equi-flux footprint on the ground. There are studies on finding the optimal steering angle (downtilt) for base station antennas [12]–[16]. This downtilt can improve energy efficiency [12], area spectral efficiency [13], [14], and network coverage or capacity [14]–[16]. The downtilt can be achieved either mechanically or electronically. However, electrical tilt is

more popular since it can be performed remotely thus saving time and costs by removing the need for tower climbs and base station site visits [17]. Furthermore, there are methods [15], [16] that utilize dynamic antenna tilt to improve the network performance. Additionally, larger steering angles are required when the base station density increases [14], which will be a growing trend due to 5G.

Since only a limited steering range is required, the aforementioned arrays with pattern reconfigurable elements [7]–[11] instead of arrays with wide element patterns [1]–[6] are a better choice for base stations and other similar applications. Reconfigurable elements allow concentrating the radiation only in the steering range of interest, whereas elements with wide element patterns are designed to radiate equally in all directions. Thus, the element gain is possibly larger for arrays with reconfigurable elements. However, these designs have been achieved through laborious electromagnetic simulations, and most of them require tuning components thus increasing complexity, introducing additional losses, and potentially causing distortion.

The numerical electromagnetics community has established systematic computational methods considering the radiation pattern or its derivatives (such as directivity) as part of antenna design [18]–[20]. However, these methods are based on finding the optimal surface current distribution of the antenna, which in practice is often difficult to realize.

We propose a novel method enabling the design of a multi-port antenna element with the desired radiation pattern by determining optimal port currents rather than optimal surface currents. The actual realization of the port currents is straightforward as the practical demonstration shows. The desired radiation pattern can be designed for maximal gain in a certain direction or for the best gain coverage over a certain angular range. In this paper, we choose to demonstrate this method by designing the radiation pattern of an array element according to the steering-range requirements of the base station antennas described and use the element to build a linear array. The effectiveness of the method is verified by comparing it to a reference antenna element, and array through simulations and measurements.

II. METHOD AND THEORY

The basis of the method is introduced in [21], where, for example, a rectangular metallic radiating region is divided into multiple closely-spaced patches. Each patch has a feeding port, and the neighboring patches are connected to each other through feeding ports as well. This multi-port structure is simulated, and the resulting scattering parameters and port-specific electric fields are then used to solve the port currents maximizing the radiation efficiency.

In this paper, we aim to maximize the partial radiation efficiency, while systematically accounting for matching as well. The difference between these two efficiencies is that radiation efficiency accounts for radiated power in a full solid angle, whereas partial radiation efficiency accounts for that in a partial solid angle. In other words, radiation efficiency is a measure of how effectively an antenna radiates overall, whereas partial radiation efficiency defines how well an antenna radiates in a certain angular range. As is the case in the base station antennas and also generally in antenna arrays backed with a ground plane, for example, the radiated power is useful only in a certain angular range. Typically, the radiation towards the back side is considered unwanted, and the goal is to maximize the radiated power in a solid angle covering at most half a sphere. Hence, the partial radiation efficiency is a better figure-of-merit in these cases than the traditional radiation efficiency.

The radiation efficiency of an N-port multi-feed antenna can be calculated with the following formula [21]:

$$\eta_{\text{rad}} = \frac{P_{\text{rad}}}{P_{\text{acc}}} = 2\frac{\boldsymbol{I}^{\text{H}}\mathbf{R}_{\text{rad}}\boldsymbol{I}}{\boldsymbol{I}^{\text{H}}\left(\mathbf{Z}_{\text{A}}^{\text{H}} + \mathbf{Z}_{\text{A}}\right)\boldsymbol{I}}, \tag{1}$$

where P_{rad} is radiated power, P_{acc} is power accepted by antenna, $\boldsymbol{I}$ is a column vector of length N containing complex port currents, $\mathbf{R}_{\text{rad}}$ is the radiation matrix of size $N \times N$, $\mathbf{Z}_{\text{A}}$ is the antenna impedance matrix of size $N \times N$, and $^{\text{H}}$ denotes the Hermitian transpose. The radiation matrix is defined as

$$(\mathbf{R}_{\text{rad}})_{\text{mn}} = \frac{1}{\eta_0}\oint_{\Omega_{4\pi}} \vec{\boldsymbol{K}}_{\text{m}}^{*}(\theta,\phi)\cdot\vec{\boldsymbol{K}}_{\text{n}}(\theta,\phi)\text{d}\Omega, \tag{2}$$

where $\vec{\boldsymbol{K}}_{\text{k}}(\theta,\phi)$ is a vector associating current i_k at port k to the far field. Since (1) has the form of a Rayleigh quotient, the port currents maximizing the radiation efficiency can be solved from the following generalized eigenvalue problem [21]:

$$\eta_{\text{rad,max}} = 2\max\left\{\text{eig}\left(\mathbf{R}_{\text{rad}}, \mathbf{Z}_{\text{A}}^{\text{H}} + \mathbf{Z}_{\text{A}}\right)\right\}. \tag{3}$$

In this paper, we modify the radiation matrix to maximize the partial radiation efficiency in solid angle $\tilde{\Omega}$ instead of the full solid angle $\Omega_{4\pi}$. We denote this new radiation matrix, having the same form as in (2), as $\mathbf{R}_{\text{rad},\tilde{\Omega}}$, and the integrating region is $\tilde{\Omega}$ instead of $\Omega_{4\pi}$. The port currents $i_{\text{max},k}$, where k is the port number, inducing the maximum partial radiation efficiency over solid angle $\tilde{\Omega}$ can be solved similarly as in the case of the full solid angle. In our case, $\mathbf{R}_{\text{rad}}$ is replaced with $\mathbf{R}_{\text{rad},\tilde{\Omega}}$ in (3).

Since we only maximize the partial radiation efficiency in solid angle $\tilde{\Omega}$, the matching network must be designed to conjugately match the chosen port impedances Z_0^k to the active port impedances Z_{in}^k to ensure a good total efficiency as well. When the port currents $i_{\text{max},k}$ are solved from the modified (3), the port voltages $u_{\text{max},k}$ are also known based on the antenna impedance matrix $\mathbf{Z}_{\text{A}}$. Hence, the active port impedance for port k can be calculated as

$$Z_{\text{in}}^k = \frac{u_{\text{max},k}}{i_{\text{max},k}} = \frac{\sum_{n=1}^{N} Z_{\text{A},kn}\cdot i_{\text{max},n}}{i_{\text{max},k}}. \tag{4}$$

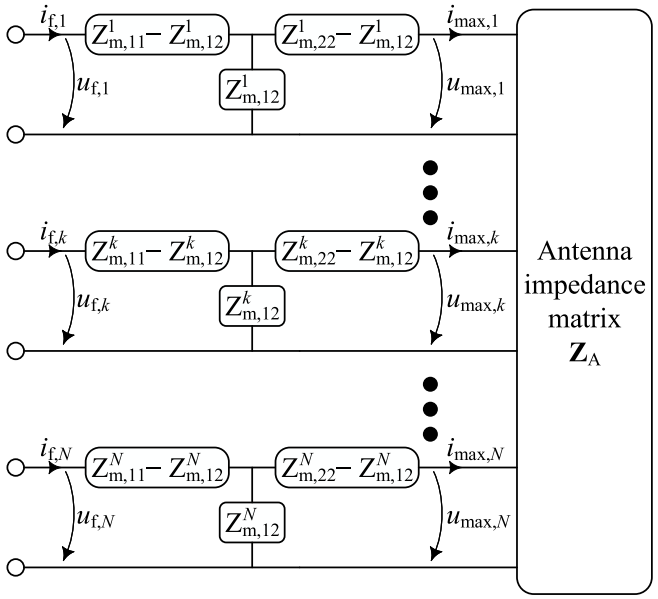

FIGURE 1. Schematic representation of voltages and currents on either side of the matching network for the *N*-port antenna.

Since the port voltage and thus the active port impedance of a multi-port antenna depends on the coupling parameters, the coupling between the ports is inherently accounted for when each port is matched to the active port impedance.

Although the antenna is fed simultaneously through multiple ports, every port can be matched separately when port currents and voltages are known. Fig. 1 shows the schematic presentation of the matching networks and the antenna with the previously determined currents $i_{\mathrm{max},k}$. The matching network of port k is expressed as an equivalent circuit based on its 2×2 impedance matrix $\mathbf{Z}_{\mathrm{m}}^{k}$. Since the currents at the antenna inputs are fixed, the active input impedances are also fixed regardless of the changes in the matching networks of the ports. Thus, each port can be separately matched to the input impedance given by (4).

After the matching networks have been determined, the remaining task is to find feeding signals that fulfill currents $i_{\mathrm{max},k}$ at antenna inputs. The feeding signal at port k is

$$a_{\mathrm{f},k} = \frac{u_{\mathrm{f},k} + Z_0^k i_{\mathrm{f},k}}{2\sqrt{\mathrm{Re}\{Z_0^k\}}}, \tag{5}$$

where $i_{\mathrm{f},k}$ and $u_{\mathrm{f},k}$ are the feeding current and voltage, respectively. Based on Fig. 1, we can solve how feeding current $i_{\mathrm{f},k}$, and voltage $u_{\mathrm{f},k}$ depend on $i_{\mathrm{max},k}$ and $u_{\mathrm{max},k}$. Voltage $u_{\mathrm{max},k}$ is expressed as

$$u_{\mathrm{max,k}} = -i_{\mathrm{max},k}\left(Z_{\mathrm{m},22}^k - Z_{\mathrm{m},12}^k\right) + Z_{\mathrm{m},12}^k\left(i_{\mathrm{f},k} - i_{\mathrm{max},k}\right), \tag{6}$$

which can be used to solve the feeding current:

$$i_{\mathrm{f},k} = \frac{1}{Z_{\mathrm{m},12}^k} u_{\mathrm{max},k} + \frac{Z_{\mathrm{m},22}^k}{Z_{\mathrm{m},12}^k} i_{\mathrm{max},k}. \tag{7}$$

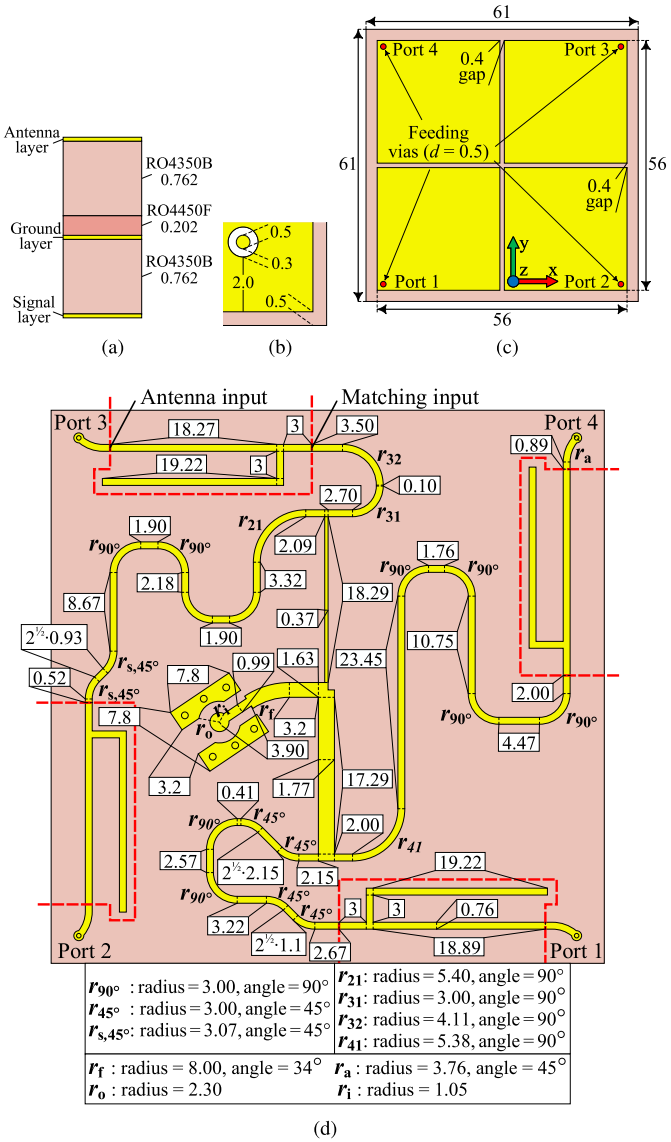

FIGURE 2. Cross-section (a) and layers (ground (b), antenna (c), and signal (d)) of the proposed antenna. All dimensions are in millimetres.

The feeding voltage $u_{\mathrm{f},k}$ is

$$\begin{aligned} u_{\mathrm{f},k} &= i_{\mathrm{f},k}\left(Z_{\mathrm{m},11}^k - Z_{\mathrm{m},12}^k\right) + Z_{\mathrm{m},12}^k\left(i_{\mathrm{f},k} - i_{\mathrm{max},k}\right) \\ &= \frac{Z_{\mathrm{m},11}^k}{Z_{\mathrm{m},12}^k} u_{\mathrm{max},k} + \frac{Z_{\mathrm{m},22}^k Z_{\mathrm{m},11}^k}{Z_{\mathrm{m},12}^k} i_{\mathrm{max},k} - Z_{\mathrm{m},12}^k i_{\mathrm{max},k}. \end{aligned} \tag{8}$$

III. DESIGN OF A SINGLE ANTENNA ELEMENT

For conventional array elements, the goal is either to achieve a wide element pattern in order to guarantee a larger beam-steering range or to design an element with a narrow beam to maximize the array performance in the broadside direction. However, we aim to maximize the array performance in a pre-defined angular space by feeding a single multi-port element with proper feeding signals. We use the modified (3) to maximize partial radiation efficiency at 2.5 GHz in the following angular space: $\theta = [0°, 90°]$ and $\phi = [-45°, 45°]$.

The proposed structure, shown in Fig. 2, consists of a 0.202-mm thick RO4450F substrate sandwiched between two

TABLE 1. Port currents, port voltages and active port impedances.

Port	Current (mA)	Voltage (V)	Impedance (Ω)
1	$63.37\angle -179.7°$	$11.83\angle -105.2°$	$49.6 + \text{j}179.9$
2	$26.30\angle +86.7°$	$5.88\angle +160.4°$	$62.9 + \text{j}214.4$
3	$28.46\angle -90.9°$	$6.18\angle -18.0°$	$63.7 + \text{j}207.4$
4	$65.36\angle +0.0°$	$12.19\angle +75.0°$	$48.1 + \text{j}180.2$

TABLE 2. Feeding signal $a_{\text{f},k}/a_{\text{f},3}$ values.

Port	Value
1	$1.96\angle -85.9°$
2	$0.92\angle -179.4°$
3	$1.00\angle +0.0°$
4	$2.00\angle +94.0°$

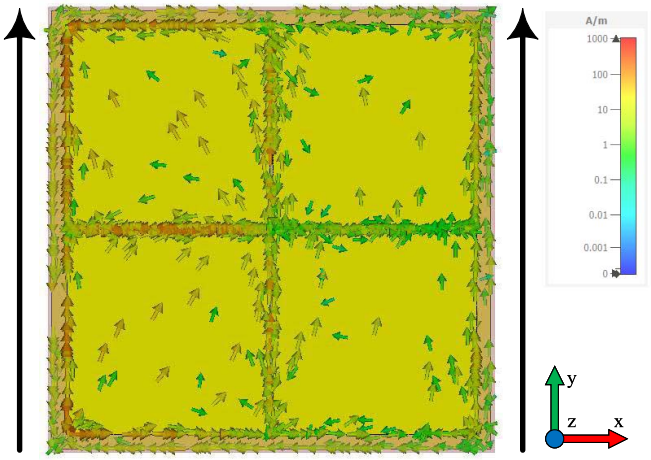

FIGURE 3. Current distribution of the proposed antenna element at 2.5 GHz.

0.762-mm thick RO4350B substrates. The antenna element comprises four closely-spaced metallic square patches each fed with a via from the outer corner. Each square patch is 0.4 mm apart from the other, and their overall size is 56 mm × 56 mm, whereas the ground plane size is 60 mm × 60 mm, corresponding to the half-wave length at the design frequency of 2.5 GHz. The substrate is extended by 0.5 mm in all directions to ease the manufacturing process. The separation between the patches and the ground is 0.964 mm. Fig. 2(d) shows the feeding side of the antenna structure that consists of four matching networks and one feeding network. The microstrip line section between the antenna and matching input in the figure is considered to be the matching network. The remaining microstrip lines form the feeding network that reduces the initial four-port feed to a single-port feed that is fed with a surface-mount SMA connector.

These networks are obtained as follows. First, the antenna structure is simulated without the networks such that each patch is fed through a separate port located at the antenna input in accordance with Fig. 2(d). The simulated impedance matrix and element patterns are used in the modified (3) to obtain the port currents that maximize the partial radiation efficiency in the pre-defined angular space. After this, the port currents are used to determine the active port impedances and voltages. These are shown in Table 1.

Then, microstrip matching networks are implemented to match the active port impedances to the feeding network output impedances, which is around 75 Ω. Ports 1 and 4, and ports 2 and 3 use the same matching network for simplicity. This is a reasonable choice since the active port impedances are almost equal for those ports.

At this stage, (5), (7), and (8) are used to calculate the feeding signals at the input of the matching networks. Table 2 shows the feeding signal values. The majority of the energy (81%) is fed into ports 1 and 4. The phase difference between those ports is close to 180°, as is the case for ports 2 and 3.

The feeding scheme also reveals the operating principle of the proposed antenna. The four patches form a linear array comprising two differentially fed antennas. The patches fed by ports 1 and 4 form a single antenna, and the remaining patches the other. We can see that the phase difference between these two antennas is around 90°.

Before designing the feeding network, we verified with simulations that the microstrip network matches the active input impedances close to 75 Ω. When the antenna is connected to the matching network and fed with the computed signals, the active reflection coefficients vary between −38.7 dB and −27.7 dB.

The feeding network is implemented based on the signals given in Table 2. The feeding network input impedance is chosen as 50 Ω, and the proper amplitude distribution at the ports is achieved with three T-junction dividers. The first T-junction divides the power between ports 1 and 4, and 2 and 3 properly, and the remaining T-junctions divide the power equally between ports 1 and 4 or ports 2 and 3. The phase difference is achieved by varying the length of the microstrip between the matching network inputs and the divider outputs.

Fig. 3 shows the current distribution of the single antenna element with the matching and feeding network at 2.5 GHz. The strongest currents lie at the left and right edges of the element, and give a rise to y-polarized radiation. The currents between the adjacent edges of the patches are in opposite phase, and hence they cancel each other and do not contribute to the radiated power.

The proposed single-antenna element is compared to the conventional coaxially-fed patch antenna operating at 2.5 GHz, shown in Fig. 4. The reference antenna has the same substrate structure as the proposed antenna, and it is also fed with an SMA connector from the signal layer, as shown in Fig. 4(b).

The single elements are also extended to four-element arrays with the elements being along the x-axis. For the reference antenna the spacing is chosen as 0.5λ (60 mm) and for the proposed antenna it is chosen as 0.6λ (72 mm). In the proposed case, the empty 12-mm space is filled with the substrate material leading to separate ground planes for the

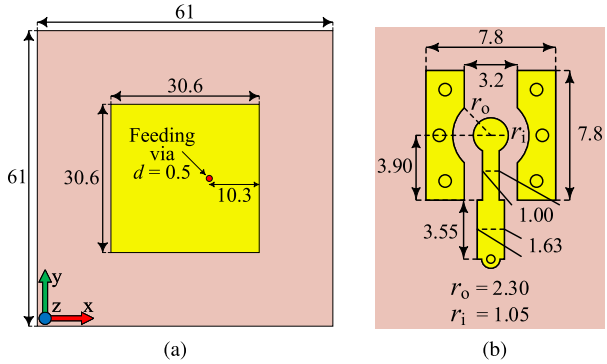

FIGURE 4. Antenna (a) and signal (b) layer of the reference antenna. All dimensions are in millimeters.

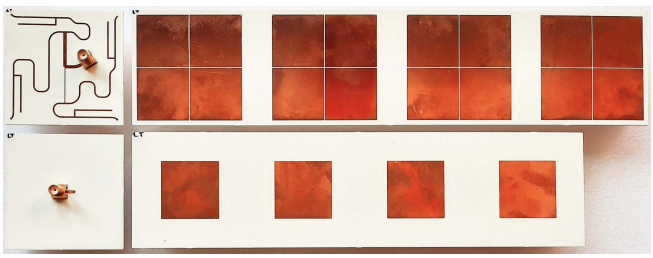

FIGURE 5. The manufactured proposed (top) and reference (bottom) antenna elements and arrays.

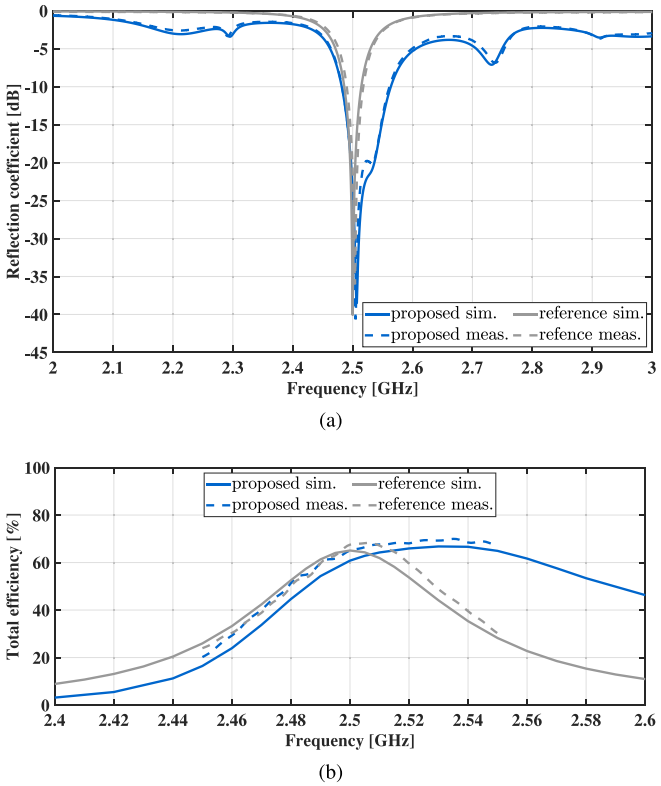

FIGURE 6. Simulated and measured reflection coefficients (a) and total efficiencies (b) of the proposed and reference single antenna element.

elements. In the reference case, the ground plane is uniform. The spacing is a little larger to mitigate the effects of the coupling for the proposed case. Whereas the conventional patch antenna array with 0.6λ inter-element spacing would result in the emergence of grating lobes at large beam steering angles, the proposed array does not. This is because the single element does not radiate in the direction of the possible grating lobes.

IV. RESULTS

In addition to simulations, both the single elements and arrays were manufactured and measured. The manufactured antennas are shown in Fig. 5. Measurements were carried out in the MVG StarLab 6-GHz system in Aalto University. The arrays were measured for element patterns, which were then numerically combined with appropriate feeding signals to determine the realized gain patterns of the arrays at different steering angles. The single-element pattern was measured by exciting a single port of the array while terminating the other ports with 50-Ω loads. Fig. 6 shows the simulated and measured reflection coefficient and total efficiency of the proposed and reference antenna element both of which agree well with each other. The figure shows that the −10 dB bandwidth is 81 MHz for the simulated proposed element which is significantly larger than that of the reference (27 MHz). Both the reference and proposed antenna elements are well matched at the design frequency since their simulated reflection coefficients at 2.5 GHz are −40 dB and −23 dB, respectively. The simulated total efficiencies of both elements are similar. The reference has a total efficiency of 65 % whereas the proposed is 4 percentage points less efficient at 2.5 GHz. However, the proposed antenna radiates more efficiently than the reference in the optimized angular space ($\theta = [0°, 90°]$ and $\phi = [-45°, 45°]$). As a figure-of-merit, we use the partial total efficiency, which is the ratio between the radiated power in the optimized angular space and the total input power. The partial total efficiency of the proposed element (23 %) is 8 percentage points higher than that of the reference.

The single-element realized gains for the proposed and reference antenna are shown in Fig. 7. The simulated reference antenna main lobe is pointed directly upwards and has a magnitude of 4.8 dBi. The magnitude of the simulated main lobe is also the same for the proposed antenna. However, the beam is tilted by about 28 degrees towards the x-axis. This is more evident in Fig. 8 that shows the cuts of the realized gain at $\phi = 0°$ and $\theta = 28°$. The proposed antenna has a physically larger aperture than the reference, allowing steering the beam away from the broadside direction while maintaining a realized gain almost equal to the reference. The figure shows that most of the radiation is directed towards the pre-defined angular space of $\theta = [0°, 90°]$ for the proposed case, and that the proposed element radiates more effectively in the range $\phi = [-45°, 45°]$ than the reference. The side lobe levels of the reference and proposed antenna are also similar. The level of both antennas is less than −15 dB. As can be seen

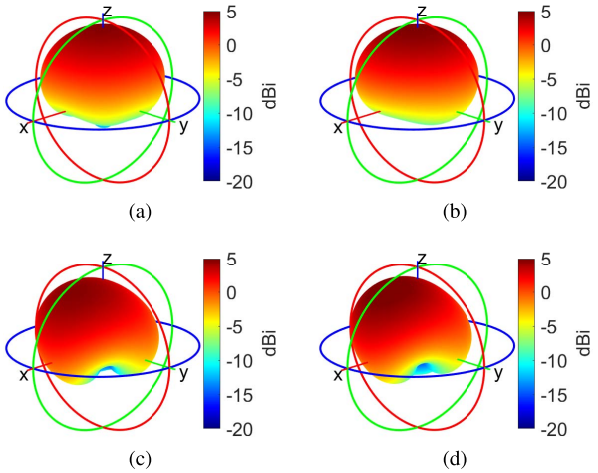

FIGURE 7. 3D radiation patterns of the simulated (a) and measured (b) reference, and simulated (c) and measured (d) proposed antenna.

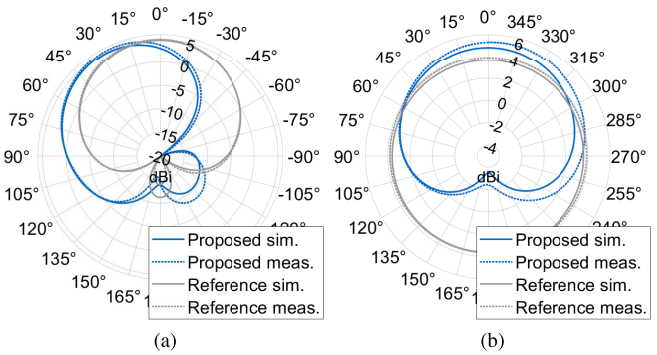

FIGURE 8. Simulated and measured realized gain pattern cuts at $\phi = 0°$ (a) and $\theta = 28°$ (b) of the reference and proposed antenna.

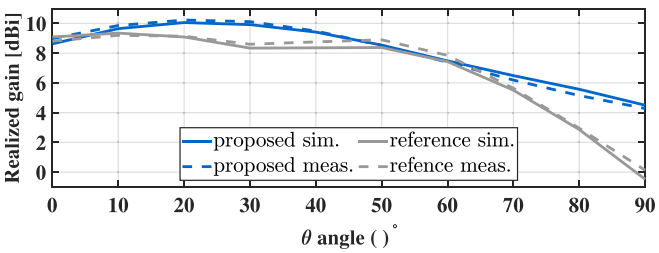

FIGURE 9. Simulated and measured realized gains of the proposed and reference antenna array as a function of the optimized steering angle.

from Figs. 7 and 8, the measurements agree well with the simulations.

The simulated and measured results for the arrays are shown in Figs. 9–11. Both arrays are steered in the xz-plane in the $\theta = [0°, 90°]$ direction. The feeding signals for different steering angles are calculated by maximizing the realized gain of the array at the corresponding steering angle using the presented method with slight modifications. The feeding signals are calculated for simulated arrays, and they are also used for their measured counterparts. The figures show that the measurement results agree well with the simulated ones.

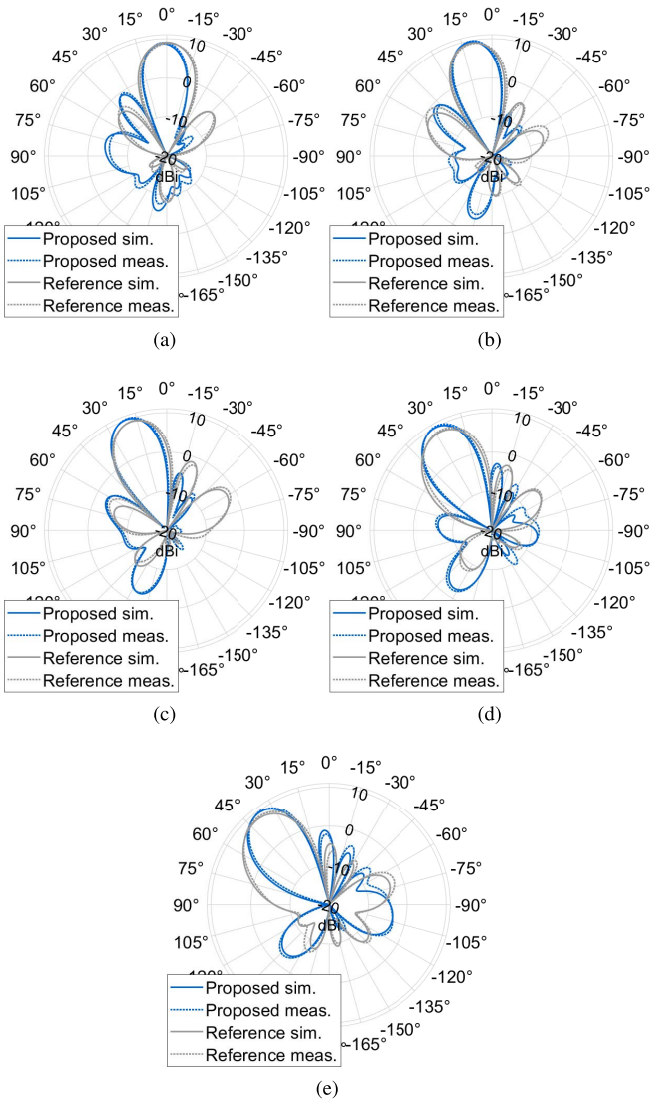

FIGURE 10. Simulated and measured realized gains of the reference and proposed array in the xz-plane when the steering angle is optimized for (a) 0°, (b) 10°, (c) 20°, (d) 30°, and (e) 40°.

Mathematically, the realized gain can be maximized by replacing $\mathbf{R}_{\text{rad}}$ and $\mathbf{Z}^{\text{H}}+\mathbf{Z} = \mathbf{Z}_{\text{acc}}^{\text{H}}\mathbf{Z}_{\text{acc}}$ in (3) with new matrices to obtain a new modification. Matrix $\mathbf{R}_{\text{rad}}$ is replaced with matrix $\mathbf{R}_{\text{rad}}^{\theta_0,\phi_0}$ computed at a single steering angle $\theta = \theta_0$ and $\phi = \phi_0$. Since the product $\boldsymbol{I}^{\text{H}}\mathbf{Z}_{\text{acc}}^{\text{H}}\mathbf{Z}_{\text{acc}}\boldsymbol{I}$ is proportional to the power accepted by the antenna, we must replace $\mathbf{Z}_{\text{acc}}$ with $\mathbf{Z}_{\text{tot}}$ so that the product is proportional to the total input power. This guarantees that the realized gain is maximized in this modified (3). The total input power is proportional to the product $\boldsymbol{a}^{\text{H}}\boldsymbol{a}$, where $\boldsymbol{a}$ is a column vector of length N containing the port feeding signals a_k of the array elements. This vector can be defined in terms of port currents as

$$\boldsymbol{a} = \frac{1}{2}\mathbf{F}(\boldsymbol{U} + \mathbf{Z}_{\text{P}}\boldsymbol{I}) = \frac{1}{2}\mathbf{F}(\mathbf{Z}_{\text{A}} + \mathbf{Z}_{\text{P}})\boldsymbol{I} = \mathbf{Z}_{\text{tot}}\boldsymbol{I}, \qquad (9)$$

where both $\mathbf{F}$ and $\mathbf{Z_0}$ are diagonal matrices of size $N \times N$, where $F_{kk} = (\sqrt{\text{Re}\{Z_0^k\}})^{-1}$, and $Z_{\text{P},kk} = Z_0^k$.

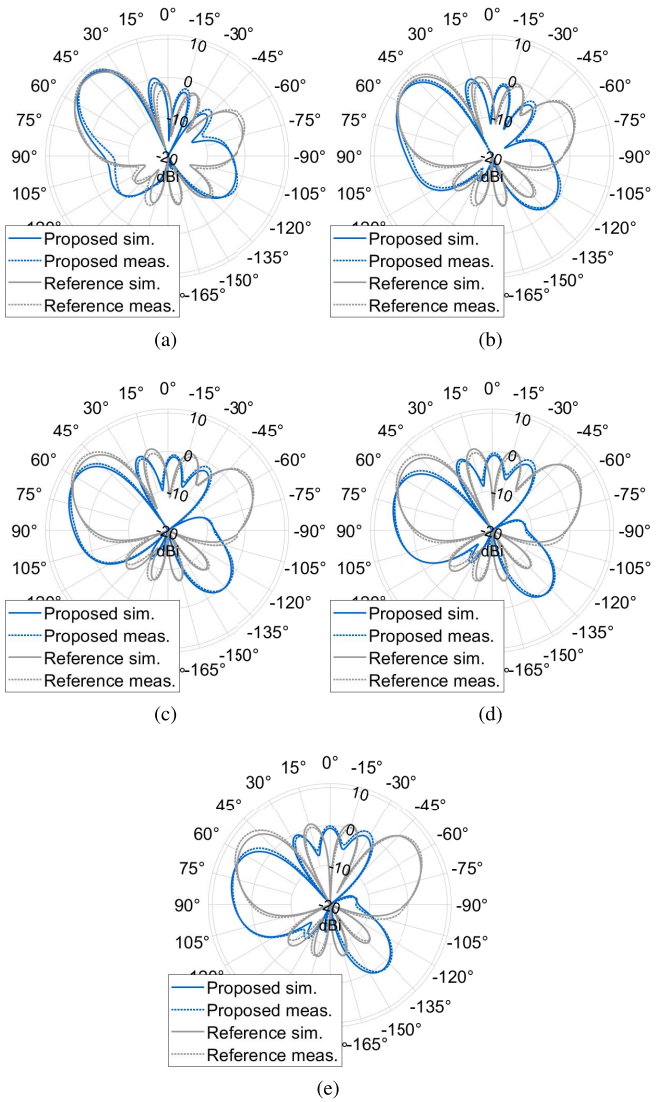

FIGURE 11. Simulated and measured realized gains of the reference and proposed array in the xz-plane when the steering angle is optimized for (a) 50°, (b) 60°, (c) 70°, (d) 80°, and (e) 90°.

Port impedance Z_0^k is 50 Ω for all the elements in both the proposed and reference arrays. Note that (9) is a vectorized form of (5). When the currents maximizing the realized gain are solved, (9) can be used to determine the values of the feeding signals for the array elements.

The results for the realized gains are shown in Fig. 9. The simulated realized gain of the proposed array is slightly lower in direction $\theta = 0°$ than for the reference case. This is a natural result, since the reference element pattern points towards the z-axis whereas the proposed element pattern does not. Other than at $\theta = 0°$, the realized gain of the proposed antenna is better. The greatest benefits are seen at large steering angles. For example at $\theta = 90°$, the realized gain is nearly 5 dB better for the proposed case.

Figs. 10 and 11 show the realized gain patterns of the reference and proposed array in the xz-plane when the steering angle is optimized for different angles. Note that when the steering angle is optimized for 40° or less, the mainlobe is approximately in the direction of the steering angle. At larger angles, the mainlobe direction is not that of the optimized steering angle since better realized gain is achieved by smaller mainlobe angle. The figures show the effects of the tilted element pattern on the array pattern. At 0°, the proposed array pattern is not symmetric as in the case of the reference. When the steering angle is 30°, the main beam of the proposed array is narrower and the peak value is greater than for the reference array. The gain patterns optimized for 90° show that, in the reference case, a grating lobe exists at the opposite angle θ that does not exist in the proposed case even though the element spacing is 0.6λ.

V. CONCLUSION

In this paper, we introduce a method to design a multi-port antenna element having the radiation pattern as the design goal, and we show how the appropriate feeding signals, and matching can be found. The advantage and design process of the method was demonstrated with simulations and measurements. The element designed with the method radiates more effectively in the desired angular space than the reference. Compared to the reference, the performance of the proposed array increases most at larger steering angles while maintaining an almost equal performance at smaller angles. In the future, the aim is to develop a method to design this single element as part of an antenna array to further improve the operation. The challenge in the future approach is finding a systematic approach to include the effects of the neighboring elements in the design process.

REFERENCES

[1] Y.-Q. Wen, B.-Z. Wang, and X. Ding, "A wide-angle scanning and low sidelobe level microstrip phased array based on genetic algorithm optimization," *IEEE Trans. Antennas Propag.*, vol. 64, no. 2, pp. 805–810, Feb. 2016.

[2] Y.-F. Cheng, X. Ding, W. Shao, M.-X. Yu, and B.-Z. Wang, "2-D planar wide-angle scanning-phased array based on wide-beam elements," *IEEE Antennas Wireless Propag. Lett.*, vol. 16, pp. 876–879, 2017.

[3] C.-M. Liu, S. Xiao, and X.-L. Zhang, "A compact, low-profile wire antenna applied to wide-angle scanning phased array," *IEEE Antennas Wireless Propag. Lett.*, vol. 17, pp. 389–392, 2018.

[4] Y.-Q. Wen, S. Gao, B.-Z. Wang, and Q. Luo, "Dual-polarized and wide-angle scanning microstrip phased array," *IEEE Trans. Antennas Propag.*, vol. 66, no. 7, pp. 3775–3780, Jul. 2018.

[5] G. Yang, Q. Chen, J. Li, S. Zhou, and Z. Xing, "Improving wide-angle scanning performance of phased array antenna by dielectric sheet," *IEEE Access*, vol. 7, pp. 71897–71906, 2019.

[6] B.-F. Sun, X. Ding, Y.-F. Cheng, and W. Shao, "2-D wide-angle scanning phased array with hybrid patch mode technique," *IEEE Antennas Wireless Propag. Lett.*, vol. 19, pp. 700–704, 2020.

[7] S. Xiao, C. Zheng, M. Li, J. Xiong, and B.-Z. Wang, "Varactor-loaded pattern reconfigurable array for wide-angle scanning with low gain fluctuation," *IEEE Trans. Antennas Propag.*, vol. 63, no. 5, pp. 2364–2369, May 2015.

[8] X. Ding, Y.-F. Cheng, W. Shao, and B.-Z. Wang, "A wide-angle scanning phased array with microstrip patch mode reconfiguration technique," *IEEE Trans. Antennas Propag.*, vol. 65, no. 9, pp. 4548–4555, Sep. 2017.

[9] G.-F. Gao, X. Ding, Y.-F. Cheng, and W. Shao, "Dual-polarized wide-angle scanning phased array based on mutimode patch elements," *IEEE Antennas Wireless Propag. Lett.*, vol. 18, no. 3, pp. 546–550, Mar. 2019.

[10] B. Ahn, I. Hwang, K.-S. Kim, S.-C. Chae, J.-W. Yu, and H. L. Lee, "Wide-angle scanning phased array antenna using high gain pattern reconfigurable antenna elements," *Sci. Rep.*, vol. 9, no. 18391, pp. 1–9, 2019.

[11] Z. Chen, Z. Song, H. Liu, X. Liu, J. Yu, and X. Chen, "A compact phase-controlled pattern-reconfigurable dielectric resonator antenna for passive wide-angle beam scanning," *IEEE Trans. Antennas Propag.*, early access, Nov. 25, 2020, doi: 10.1109/TAP.2020.3030549.

[12] B. Badic, T. O'Farrell, P. Loskot, and J. He, "Effect of the base station antenna beam tilting on energy consumption in cellular networks," in *Proc. IEEE 72nd Veh. Technol. Conf. Fall*, 2010, pp. 1–5.

[13] X. Li, R. W. Heath, K. Linehan, and R. Butler, "Metrocell antennas: The positive impact of a narrow vertical beamwidth and electrical downtilt," *IEEE Veh. Technol. Mag.*, vol. 10, no. 3, pp. 51–59, Sep. 2015.

[14] J. Yang, M. Ding, G. Mao, Z. Lin, D.-G. Zhang, and T. H. Luan, "Optimal base station antenna downtilt in downlink cellular networks," *IEEE Trans. Wireless Commun.*, vol. 18, no. 3, pp. 1779–1791, Mar. 2019.

[15] A. Engels, M. Reyer, X. Xu, R. Mathar, J. Zhang, and H. Zhuang, "Autonomous self-optimization of coverage and capacity in LTE cellular networks," *IEEE Trans. Veh. Technol.*, vol. 62, no. 5, pp. 1989–2004, Jun. 2013.

[16] V. Buenestado, M. Toril, S. Luna-Ramirez, J. M. Ruiz-Aviles, and A. Mendo, "Self-tuning of remote electrical tilts based on call traces for coverage and capacity optimization in LTE," *IEEE Trans. Veh. Technol.*, vol. 66, no. 5, pp. 4315–4326, May 2017.

[17] O. N. C. Yilmaz, S. Hamalainen, and J. Hamalainen, "Comparison of remote electrical and mechanical antenna downtilt performance for 3GPP LTE," in *Proc. IEEE 70th Veh. Technol. Conf. Fall*, 2009, pp. 1–5.

[18] M. Gustafsson and S. Nordebo, "Optimal antenna currents for Q, superdirectivity, and radiation patterns using convex optimization," *IEEE Trans. Antennas Propag.*, vol. 61, no. 3, pp. 1109–1118, Mar. 2013.

[19] M. Gustafsson, J. Friden, and D. Colombi, "Antenna current optimization for lossy media with near-field constraints," *IEEE Antennas Wireless Propag. Lett.*, vol. 14, pp. 1538–1541, 2015.

[20] M. Gustafsson and M. Capek, "Maximum gain, effective area, and directivity," *IEEE Trans. Antennas Propag.*, vol. 67, no. 8, pp. 5282–5293, Aug. 2019.

[21] R. Kormilainen, J.-M. Hannula, T. O. Saarinen, A. Lehtovuori, and V. Viikari, "Realizing optimal current distributions for radiation efficiency in practical antennas," *IEEE Antennas Wireless Propag. Lett.*, vol. 19, pp. 731–735, 2020.